CrossMark

ORIGINAL ARTICLE

Exponential leap-forward gradient scheme for determining the isothermal layer depth from profile data

Peter C. Chu[1] · Chenwu Fan[1]

Abstract Two distinct layers usually exist in the upper ocean. The first has a near-zero vertical gradient in temperature (or density) from the surface and is called the isothermal layer (or mixed layer). Beneath that is a layer with a strong vertical gradient in temperature (or density), called the thermocline (or pycnocline). The isothermal layer depth (ILD) or mixed layer depth (MLD) for the same profile varies depending on the method used to determine it. Also, whether they are subjective or objective, existing methods of determining the ILD do not estimate the thermocline (pycnocline) gradient. Here, we propose a new exponential leap-forward gradient (ELG) method of determining the ILD that retains the strengths of subjective (simplicity) and objective (gradient change) methods and avoids their weaknesses (subjective methods are threshold-sensitive and objective methods are computationally intensive). This new method involves two steps: (1) the estimation of the thermocline gradient G_{th} for an individual temperature profile, and (2) the computation of the vertical gradient by averaging over gradients using exponential leap-forward steps. Such averaging can filter out noise in the profile data. Five existing methods of determining the ILD (difference, gradient, maximum curvature, maximum angle, and optimal linear fitting methods) as well as the proposed ELG method were verified using global expendable bathythermograph (XBT) temperature and conductivity–temperature–depth (CTD) datasets. Among all the methods considered, the ELG method yielded the highest skill score and the lowest Shannon information entropy (i.e., the lowest uncertainty).

Keywords Mixed layer · Mixed layer depth · Isothermal layer · Isothermal layer depth · Difference · Gradient · Maximum curvature · Maximum angle · Optimal linear fitting · Exponential leap-forward gradient (ELG) · Quality index · Skill score · Shannon information entropy

1 Introduction

Near the ocean surface, intense turbulent mixing driven by shear (due to surface wind stress) and convection (due to heat loss from the ocean to the atmosphere) leads to a layer that is vertically quasi-uniform (i.e., has a near-zero vertical gradient) in temperature and density. Depending on whether the temperature or the density is being studied, this layer is termed the isothermal layer or the mixed layer, respectively. Beneath the isothermal (mixed) layer, there is a layer—the thermocline (for temperature) or the pycnocline (for density)—with a strong vertical gradient that restricts heat (buoyancy) exchange between the isothermal (mixed) layer and the deep layer below the thermocline/pycnocline (Fig. 1).

The isothermal (mixed) layer provides dynamic–thermodynamic links and mediates the exchange of mass, momentum, and heat between the atmosphere and the ocean; it is therefore a influence on the weather and the climate. This exchange depends on an important parameter, the isothermal layer depth (ILD, H_T) [or the mixed layer depth (MLD, H)], which determines the heat content and mechanical inertia of the layer. Temporal variability in H_T (or H) is caused by many processes that occur in the isothermal

✉ Peter C. Chu
pcchu@nps.edu

Chenwu Fan
fan@nps.edu

[1] Naval Ocean Analysis and Prediction Laboratory, Department of Oceanography, Naval Postgraduate School, 1 University Circle, Monterey, CA 93940, USA
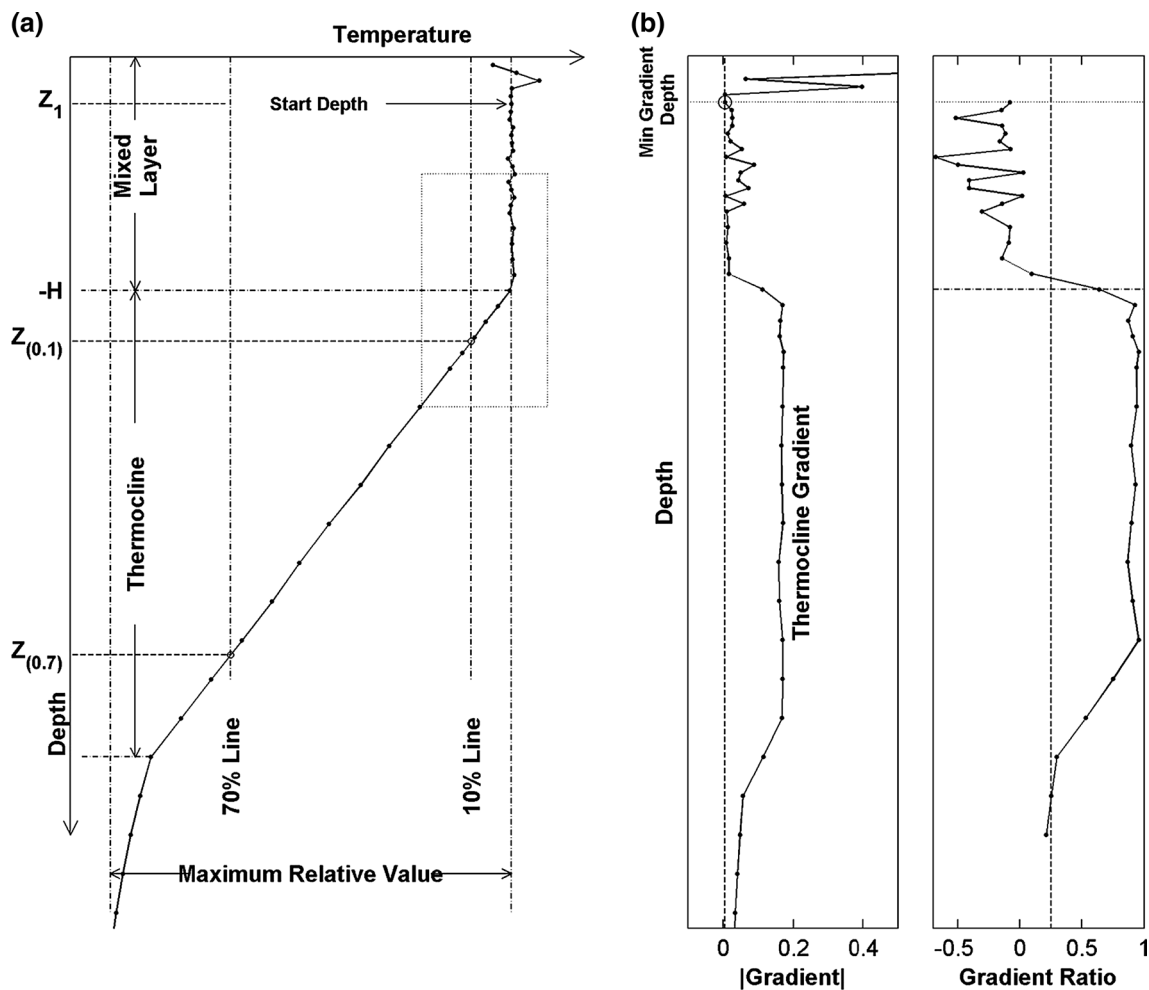
Fig. 1 Characteristics of the mixed layer and thermocline: **a** temperature profile illustrating the depths $z_{(0.1)}$ and $z_{(0.7)}$; **b** the vertical gradient $\partial T/\partial z$ and the definition of z_1

(mixed) layer (surface forcing, lateral advection, internal waves, etc.); such variability is diurnal, seasonal, and interannual (e.g., Chu 1993; Chu et al. 1990, Chu and Garwood 1991). Spatial variability in H_T (or H) ranges from less than 20 m in summer to more than 500 m in winter at subpolar latitudes (Monterey and Levitus 1997).

Table 1 gives examples of the various methods/criteria that have been used to determine the ILD from the temperature profile. A single-gradient (near-zero) concept is often used to determine H_T. The difference method requires the deviation of T from its value at a reference depth (z_{ref}) to be smaller than a certain fixed threshold value. The threshold applied varies from 1.0 °C (Lamb 1984; Rao et al. 1989; Obata et al. 1996) to 0.8 °C (Kara et al. 2000), 0.5 °C (Wyrtki 1964), 0.2 °C (de Boyer Montegut et al. 2004; Oka et al. 2007; Chu and Fan 2010a, b), and 0.1 °C (Sprintall and Roemmich 1999). The reference level used varies from near to the surface (Wyrtki 1964) to a depth of 10 m (de Boyer Montegut et al. 2004; Sprintall and Roemmich

1999). Kara et al. (2000) claimed that 0.8 °C is the optimal criterion after performing a statistical comparison between data in the NOAA National Centers for Environmental Information (NCEI) World Ocean Atlas (WOA) and a long-term time series of monthly ocean weather station observations.

The gradient method requires $\partial T/\partial z$ to be smaller than a certain fixed value. This value has varied from 0.015 °C/m (Defant 1961) to 0.02 °C/m (Wyrtki 1964), and ≥ 0.025 °C/m (Lukas and Lindstrom 1991; Chu et al. 2002). A dual-gradient (changing from a near-zero to a non-zero gradient) concept is also used to determine H_T. For example, taking the curvature to be largest at $-H_T$ (Fig. 1), i.e.,

$$z = -H_T, \left| \partial^2 T/\partial z^2 \right| \to \max, \tag{1}$$

leads to the maximum curvature method (Chu et al. 1997, 1999, 2000; Lorbacher et al. 2006). However, as pointed out by Chu et al. (1999) and Chu (2006), large errors may

Table 1 List of methods of determining the ILD from a temperature profile (note: this is not a complete list)

Source	Area	Criterion/method	$-z_{ref}$	Gradient
Sprintall and Roemmich (1999)	Pacific	$\Delta T = 0.1\ °C$	10 m	Single
Oka et al. (2007)	North Pacific	$\Delta T = 0.2\ °C$	0 m	Single
Thompson (1976)	North Pacific	$\Delta T = 0.2\ °C$	3 m	Single
de Boyer Montegut et al. (2004)	Global ocean	$\Delta T = 0.2\ °C$	10 m	Single
Obata et al. (1996) Monterey and Levitus (1997)	Global ocean	$\Delta T = 0.5\ °C$	0 m	Single
Araujo et al. (2011)	Southwest tropical Atlantic	$\Delta T = 0.5\ °C$	0 m	Single
Chu et al. (2010)	Global ocean	$\Delta T = 0.8\ °C$	0 m	Single
Lamb (1984)	Tropical Atlantic	$\Delta T = 1.0\ °C$	0 m	Single
Rao et al. (1989)	Indian Ocean	$\Delta T = 1.0\ °C$	10 m	Single
Defant (1961)	Atlantic Ocean	$\partial T/\partial z = 0.015\ °C/m$		Single
Wyrtki (1964)	East Pacific Ocean	$\partial T/\partial z = 0.02\ °C/m$		Single
Lukas and Lindstrom (1991)	Western equatorial Pacific	$\partial T/\partial z = 0.025\ °C/m$		Single
Chu et al. (1997)	Yellow Sea	Maximum curvature		Dual
Chu et al. (1999)	Beaufort/Chukchi Sea	Maximum curvature		Dual
Lorbacher et al. (2006)	Global ocean	Maximum curvature		Dual
Chu and Fan (2011)	Western North Atlantic	Maximum angle		Dual
Chu and Fan (2010a, b)	Western North Atlantic	Optimal linear fitting		Dual
This paper	Global ocean	Exponential leap-forward gradient (ELG)		Dual

occur when using this method with noisy profile data, since the curvature method involves calculating the second derivative versus depth. Therefore, to improve the curvature method, Chu and Fan (2010a, b, 2011) developed the optimal linear fitting (OLF) and maximum angle methods to identify H_T, which are capable of handling noisy profile data. However, these two methods are iterative and not as straightforward to use as methods developed previously (such as the difference, gradient, and maximum curvature methods).

Given this diversity of methods for calculating H_T, questions arise. What is the uncertainty in the results given by the existing methods/criteria? Can this uncertainty be quantified objectively? Is it possible to develop a new straightforward method that is capable of handling noisy profile data and yields H_T values with low uncertainty? The purpose of the study reported in the present paper was to answer these questions. The rest of the paper proceeds as follows. Section 2 describes the expendable bathythermograph (XBT) dataset (572,504 profiles from 1990 to 2013) from the Global Temperature and Salinity Profile Program (GTSPP) and the conductivity–temperature–depth (CTD) dataset (847,560 profiles from 1961 to 2012) from the NCEI World Ocean Database (WOD). Section 3 discusses the uncertainty associated with and the capabilities of five existing methods of determining the ILD. Section 4 presents a new, highly capable exponential leap-forward gradient (ELG) method of identifying H_T with low uncertainty. Section 5 shows the global seasonal ILD and its

statistical characteristics (such as its standard deviation, skewness, and kurtosis) that were identified by applying the ELG method to the combined GTSPP/XBT and WOD/CTD data. Section 6 shows the dynamical implications of those results. Section 7 presents the conclusions of this study. Appendices 1, 2, and 3 present MATLAB functions for computing the thermocline gradient, preparing for ELG, and determining H_T using the ELG scheme, as well as an analytical temperature profile "dataset" that can be employed to practice the use of the MATLAB functions,

$$T = T_{(\tilde{z})}. \tag{2}$$

2 Datasets

The WOD/CTD temperature (1961–2012, 847,560 profiles) and global GTSPP/XBT (1990–2013, 572,504 profiles) datasets were used to evaluate the five most commonly used methods [difference, gradient, maximum curvature, maximum angle, and optimal linear fitting (OLF)] listed in Table 1. The WOD data have been made available to the public for many years by the NOAA National Centers for Environmental Information (NCEI) through the website https://www.nodc.noaa.gov/OC5/WOD/pr_wod.html. The primary goals of the GTSPP are to develop and maintain a global ocean temperature–salinity resource containing data that are both up-to-date and of the highest possible quality, and to make global measurements of ocean temperature and salinity quickly and easily accessible to

users (Sun et al. 2010). Both real-time data (transmitted over the Global Telecommunications System, GTS) and delayed-mode data (received by the NCEI) are acquired and incorporated into a continuously managed database. The quality control procedures used in GTSPP were developed by Canada's Marine Environmental Data Service and published through the Intergovernmental Oceanographic Commission (IOC) (GTSPP Working Group 2010). Interested readers are also referred to http://www.iode.org for more detailed information. It should be noted that there is a fall-rate bias issue with older XBT probes and a pure thermal bias issue with the XBT data (Cheng et al. 2016). The GTSPP preserves XBT data, probe type, and fall-rate equation information (when provided) in the continuously managed database. Two new codes were created to retain depth correction information in the GTSPP data. Interested readers are referred to Sun et al. (2009), which can be downloaded from http://www.oceanobs09.net/proceedings/cwp/cwp86/index.php. Both the WOD/CTD and the GTSPP/XBT profiles are available in various resolutions, ranging from high (increments of about 1 m) to low (increments of much larger than 10 m).

3 Capabilities of and uncertainty associated with the existing methods

3.1 Q index

Let us represent an observational temperature profile from z_1 down to a depth z_K as $[T(z_k), k = 1, 2, …, K]$, with $\langle T \rangle$ being the vertical mean. The Q index,

$$Q = 1 - \frac{\sigma|_{-H_T}}{\sigma|_{-1.5 \times H_T}}, \qquad (3)$$

was proposed by Lorbacher et al. (2006) as a means to determine the quality of a determined value of the ILD. Here, σ is the standard deviation of $[T(z_k)]$. For a perfect determination of the ILD,

$$\sigma|_{-H_T} \cong 0, \ \sigma|_{-1.5 H_T} = \text{ finite positive value}, \qquad (4)$$

which causes $Q = 1$. When the ILD has been greatly underestimated, both H_T and $1.5 \times H_T$ are smaller than the real ILD,

$$\sigma|_{-H_T} \sim \sigma|_{-1.5 H_T} \sim \text{comparable small positive values}, \qquad (5)$$

which yields small Q values. For a greatly overestimated value of the ILD, both H_T and $1.5 \times H_T$ are larger than the real ILD,

$$\sigma|_{-H_T} \sim \sigma|_{-1.5 H_T} \sim \text{comparable finite positive values}, \qquad (6)$$

which also yields small Q values. Values for the Q index usually lie in the interval $[0, 1]$.

3.2 Skill score and Shannon information entropy

The ILD (or MLD) is well identified if $Q \geq 0.8$, uncertainly identified if $0.8 > Q \geq 0.5$, and cannot be identified if $Q < 0.5$ (Lorbacher et al. 2006). For a group of profiles (such as a temperature profile dataset), we can calculate the frequency of occurrence of Q values in each of these three intervals, i.e., $F[Q \geq 0.8]$, $F[0.8 > Q \geq 0.5]$, and $F[Q < 0.5]$. Increasing the value of $F[Q \geq 0.8]$ and decreasing the value of $F[Q < 0.5]$ improves the quality of H determination.

A skill score can be defined as

$$S = \frac{1}{2}\{1 + F[Q \geq 0.8] - F[Q < 0.5]\}, \qquad (7)$$

which represents the overall ability of a given method/criterion to accurately determine H based on a given profile dataset. If the Q values are all above 0.8 (H_T is well identified), we have $F(Q \geq 0.8) = 1$, which gives $S = 1$. If the Q values are all less than 0.5 (H_T cannot be identified), we have $F(Q < 0.5) = 1$, which leads to $S = 0$. If the Q values are between 0.8 and 0.5 (uncertain determination), we have $F(0.5 \leq Q < 0.8) = 1$, which leads to $S = 0.5$. The average of 1 and 0.5 (i.e., 0.75),

$$S \geq 0.75, \qquad (8)$$

can therefore be used as a threshold to identify a capable ILD-identification method.

Now let the interval [0, 1] be divided into J subintervals of equal size ($J = 50$ in this work), and let p_j be the frequency of occurrence of Q values in the j-th subinterval. The Shannon information entropy, which is commonly used to represent uncertainty, is defined as

$$E = -\sum_{j=1}^{J} p_j \log_2 p_j. \qquad (9)$$

The larger the Shannon information entropy, the larger the uncertainty in H_T. The five existing methods listed in Table 1 were used to calculate H_T from the WOD/CTD and GTSPP/XBT data based on various criteria, and the Q value, skill score (S), and Shannon information entropy (E) were determined in each case (see Table 2).

According to Table 2, the uncertainty associated with the subjective methods evidently varies with the dataset used. The difference method has higher S values for GTSPP/XBT (0.65–0.75) than for WOD/CTD (0.43–0.68) and lower E values for GTSPP/XBT (3.09–3.31) than for WOD/CTD (3.29–3.39); it also gives its highest S values (0.75, 0.68) and lowest E values (3.09, 3.29) with a threshold of 0.2 °C and $z_{ref} = -10$ m when using the (GTSPP/XBT, WOD/CTD) datasets. The gradient method has higher S values for WOD/CTD (0.72–0.75)

Table 2 Skill scores and Shannon information entropies of the Q index for various methods of identifying the ILD using the WOD/CTD temperature (1961–2012, 847,560 profiles) and global GTSPP/XBT (1990–2013, 572,504 profiles) datasets

Method	Criterion	$-z_{ref}$ (m)	S_{XBT}	E_{XBT}	S_{CTD}	E_{CTD}
Difference $\Delta T =$	(1) 0.1 °C	10	0.70	3.15	0.68	3.29
	(2) 0.2 °C	0	0.73	3.12	0.67	3.32
	(3) 0.2 °C	3	0.73	3.13	0.67	3.32
	(4) 0.2 °C	10	0.75*	3.09	0.68	3.29
	(5) 0.5 °C	0	0.73	3.17	0.58	3.39
	(6) 0.8 °C	0	0.69	3.26	0.49	3.45
	(7) 0.8 °C	10	0.69	3.26	0.48	3.46
	(8) 1.0 °C	0	0.66	3.30	0.44	3.49
	(9) 1.0 °C	10	0.65	3.31	0.43	3.49
Gradient $\partial T/\partial z =$	(1) 0.015 °C/m		0.60	3.25	0.72	3.03
	(2) 0.02 °C/m		0.70	3.19	0.74	3.03
	(3) 0.025 °C/m		0.70	3.15	0.75*	3.03
Max curvature			0.55	3.46	0.41	3.57
Max angle			0.74	3.12	0.76*	3.17
OLF			0.80*	2.96	0.78*	2.85
ELG			0.83*	2.88	0.82*	2.81

* The skill score is ≥ 0.75

than for GTSPP/XBT (0.60–0.70); it also gives its highest S values (0.70, 0.75) and lowest E values (3.15, 3.03) with a threshold of 0.025 °C/m when using the (GTSPP/XBT, WOD/CTD) datasets.

The objective methods yield lower uncertainty than the subjective methods, except for the maximum curvature method, which has low S values (0.55, 0.41) and high E values (3.46, 3.57) for both datasets. This is due to the calculation of the second derivative versus depth in this method. Excluding the maximum curvature method, the uncertainty associated with the objective methods varies slightly with the dataset used, i.e., the maximum angle and optimal linear fitting methods have comparably high S values for GTSPP/XBT (0.74, 0.80) and WOD/CTD (0.76, 0.78) and low E values for GTSPP/XBT (3.12, 2.96) and WOD/CTD (3.17, 2.85).

4 Exponential leap-forward gradient (ELG) method

The two objective methods (maximum angle and optimal linear fitting) have high S values and low E values but are computationally intensive since iteration is needed. Here, we introduce a new exponential leap-forward gradient (ELG) method (i.e., an extended gradient method) of determining the ILD with a noise-filtering capability. Unlike the existing methods discussed above, the ELG involves two steps: (a) the estimation of the thermocline gradient (G_{th}) and (b) the determination of the ILD using the near-zero gradient method and G_{th}.

4.1 Thermocline gradient

Usually, ocean profile datasets are noisy near the surface, with unrealistically large gradients (Fig. 1). To estimate the mixed layer gradient (near-zero) and the thermocline gradient (nonzero), it is necessary to determine the depth at which the minimum gradient occurs in the near-surface layer (z_1), i.e.,

$$\left|\frac{\Delta T}{\Delta z}\right|_{z=z_1} = \min_{z \geq -20 \text{ m}} \left|\frac{\Delta T}{\Delta z}\right|. \tag{10}$$

The near-surface layer depth (-20 m) is chosen in such a way that it is deeper than any reference levels used in the difference method (0, -3 m, -10 m; see Table 1) but is not below the thermocline. This approach reduces the effect of noise near the ocean surface.

The minimum gradient at z_1 is the best representation of the mixed-layer gradient. The vertical temperature difference from this depth (z_1) to the bottom (z_b) of the profile, $T_d = T(z_1) - T(z_b)$, is the temperature variability across the mixed layer, thermocline, and deep layer. Since the vertical gradient is strongest in the thermocline and weakest in the mixed layer, the main part of the thermocline can be considered to lie roughly between two depths, $z_{(0.1)}$ with $T(z_1) - T(z_{(0.1)}) = 0.1T_d$ and $z_{(0.7)}$ with $T(z_1) - T(z_{(0.7)}) = 0.7T_d$ (Fig. 1).

For temperature profile data that follow the pattern shown in Fig. 1a, the thermocline gradient is easily calculated as

$$G_{th} = \frac{T(z_{(0.1)}) - T(z_{(0.7)})}{z_{(0.1)} - z_{(0.7)}}. \tag{11}$$

For temperature profile data that do not follow the pattern shown in Fig. 1a (i.e., noisy data), Eq. 11 may not be representative. The data between $z_{(0.1)}$ and $z_{(0.7)}$ are rearranged into $[T_i, i = 0, 1, 2, \ldots, I]$ with $[T_0 = T(z_{(0.1)}), T_I = T(z_{(0.7)})]$. Vertical gradients are calculated between T_i ($i = 1, 2, \ldots, I$) and T_0:

$$G_i = \frac{T(z_{(0.1)}) - T_i}{z_{(0.1)} - z|_{T_i}}, \; i = 1, 2, \ldots, I.$$

The thermocline gradient (G_{th}) is estimated by finding the median of the above gradients,

$$G_{th} = \text{median}\{G_1, G_2, \ldots, G_I\}. \tag{12}$$

If the computed G_{th} is very small, i.e.,

$$G_{th} \leq 0.001 \; °C/m, \tag{13}$$

the thermocline vanishes and the mixed layer extends to the bottom of the profile (z_b). It should be noted that the gradient criterion in Eq. 13 is an order of magnitude smaller than the most commonly used gradient method listed in Table 1.

4.2 ELG scheme

Let the number of data points between z_1 and $z_{(0.7)}$ (Fig. 1) be N_g, and let $N = [\log_2(N_g)]$, with the bracket indicating the integer part of the real number inside. N is much smaller than N_g. Starting from z_1, the $(N + 1)$ exponential leap-forward gradients (ELGs) are calculated at depths z_k [between z_1 and $z_{(0.7)}$] (Fig. 2):

$$D_n T(z_k) = \frac{T(z_k) - T(z_{k+2^n})}{z_k - z_{k+2^n}}, \; n = 0, 1, 2, \ldots, N. \tag{14}$$

The average value for $(N + 1)$ gradients $[D_0 T(z_k), D_1 T(z_k), \ldots, D_N T(z_k)]$ is computed via

$$\tilde{G}(z_k) = \frac{\sum_{n=0}^{N} D_n T(z_k)}{N + 1}, \tag{15}$$

which effectively represents the gradient at depth z_k and has the ability to filter out noise in the gradient calculation. Since $\tilde{G}(z_k) \approx 0$ if z_k is in the mixed layer and $\tilde{G}(z_k) = G_{th}$ if z_k is in the thermocline, it is reasonable to use the midpoint between the two averages to separate the two layers (the mixed layer and the thermocline):

$$\tilde{G}(z_k)/G_{th} \begin{cases} < 0.5, & z_k \text{ in the mixed layer} \\ \geq 0.5, & z_k \text{ in the thermocline} \end{cases} \tag{16}$$

This method is called the exponential leap-forward gradient (ELG) method, and it yields the highest S values ($S_{XBT} = 0.83$, $S_{CTD} = 0.82$) and lowest E values ($E_{XBT} = 2.88$, $E_{CTD} = 2.81$) of any of the methods listed in Table 2.
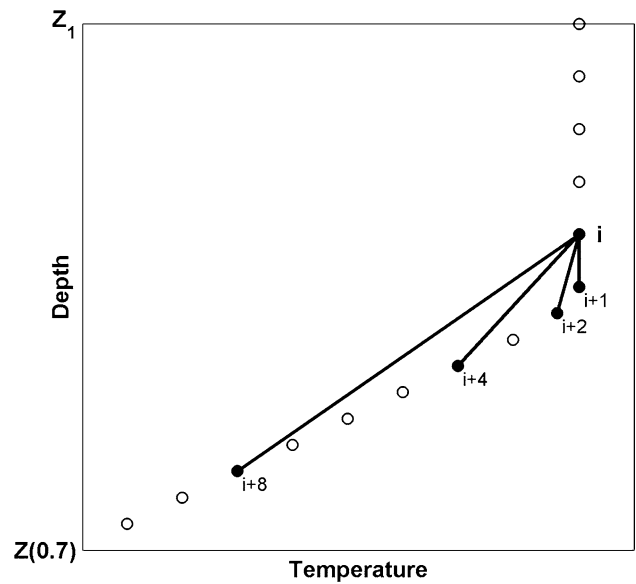
Fig. 2 Illustration of the exponential leap-forward gradient (ELG) technique

5 Global ILD dataset

A global H_T dataset was created by applying the ELG method to a combination of the GTSPP/XBT (572,504) and WOD/CTD (847,560) profile data. The H_T data were divided into four seasons: (a) January–February–March (JFM); (b) April–May–June (AMJ); (c) July–August–September (JAS); (d) October–November–December (OND). To analyze the statistics at any grid point (grid resolution: $1° \times 1°$) during the four seasons (JFM, AMJ, JAS, and OND), the H_T data in a moving grid box with its center at the grid point were considered. For each season, the mean (Fig. 3), standard deviation (Fig. 4), skewness (Fig. 5), and kurtosis (Fig. 6) of the ILD were calculated for two moving box sizes ($5° \times 5°$, $3° \times 3°$) each containing at least five data points. The lack of any noticeable difference between the left and right panels in Figs. 3, 4, 5, and 6 demonstrates that the calculated statistical parameters are not sensitive to the box size (either $5° \times 5°$ or $3° \times 3°$).

The pattern of the mean H_T (Fig. 3) is quite similar to that seen in an earlier study (Lorbacher et al. 2006), with the most prominent feature occurring throughout the year in the equatorial Pacific: negative zonal gradients with shallow H_T values (<40 m) in the east and deep H_T values (>100 m) in the west. A broad tongue of shallow H_T values occurs in the eastern equatorial Pacific during the first half of the year (Fig. 3a, b, JFM and AMJ). Such negative zonal gradients also occur in the equatorial Atlantic Ocean but they are much weaker. Evident seasonal variation is observed away from the equatorial
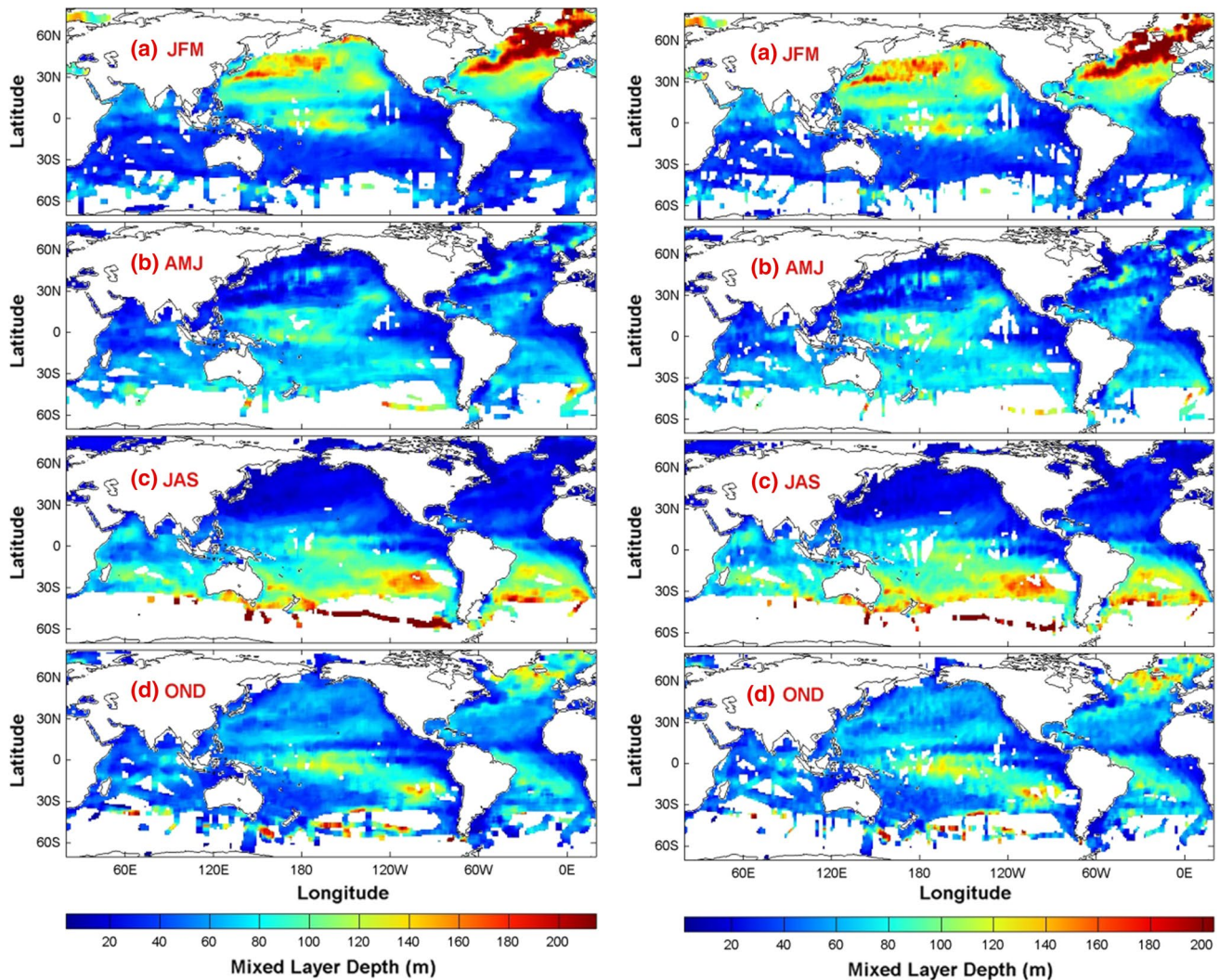
Fig. 3 Seasonal maps (1° × 1° resolution) of the mean isothermal layer depth (in meters, identified by the ELG method) averaged in moving 5° × 5° (*left panel*) and 3° × 3° (*right panel*) grid boxes and evaluated at the centers of the boxes: **a** January–February–March, **b** April–May–June, **c** July–August–September, and **d** October–November–December. *White regions* have undefined values due to the presence of insufficient data points (≤4 points) in the 5° × 5° (or 3° × 3°) grid box

regions: deep (shallow) H_T values are usually found in the North (South) Pacific and North (South) Atlantic in JFM (Fig. 3a) and vice versa in JAS (Fig. 3c). In the northwestern Pacific at around 30°N, a band with $H_T < 75$ m appears in the winter (Fig. 3a) and spring (Fig. 3b) from the west coast to 150°W, with deeper H_T values occurring around that band (Fig. 3a, b, JFM and AMJ). This is due to the occurrence of the subtropical front under which the mixed layer remains shallow, even in strong winds that produce deep mixed layers north and south of the front. This band disappears in summer (JAS) and fall (OND), when $H_T < 40$ m above about 23°N (Fig. 3c, d). In the southeastern Pacific west of Peru, a band with $H_T > 100$ m appears in the winter (JAS, Fig. 3c) near to 23°S, 100–130°W, and in spring (OND, Fig. 3d), albeit

with a much-reduced size. This band of deep H_T disappears in the summer (JFM, Fig. 3a) and fall (AMJ, Fig. 3b).

The standard deviation of H_T (Fig. 4) shows evident horizontal and seasonal variability, with weaker seasonal variation observed in the tropics (between 23°S and 23°N) than outside the tropics (north of 23°N and south of 23°S), where large values (>50 m) occur in winter and spring (JFM and AMJ in the Northern Hemisphere, JAS and OND in the Southern Hemisphere). The standard deviation of H_T is largest in the Southern Ocean in winter and spring (Fig. 4c, d) due to temporal gaps in the data. Once the seasonal thermocline has formed in the mid-latitudes, the variability of H_T is less than 10 m in
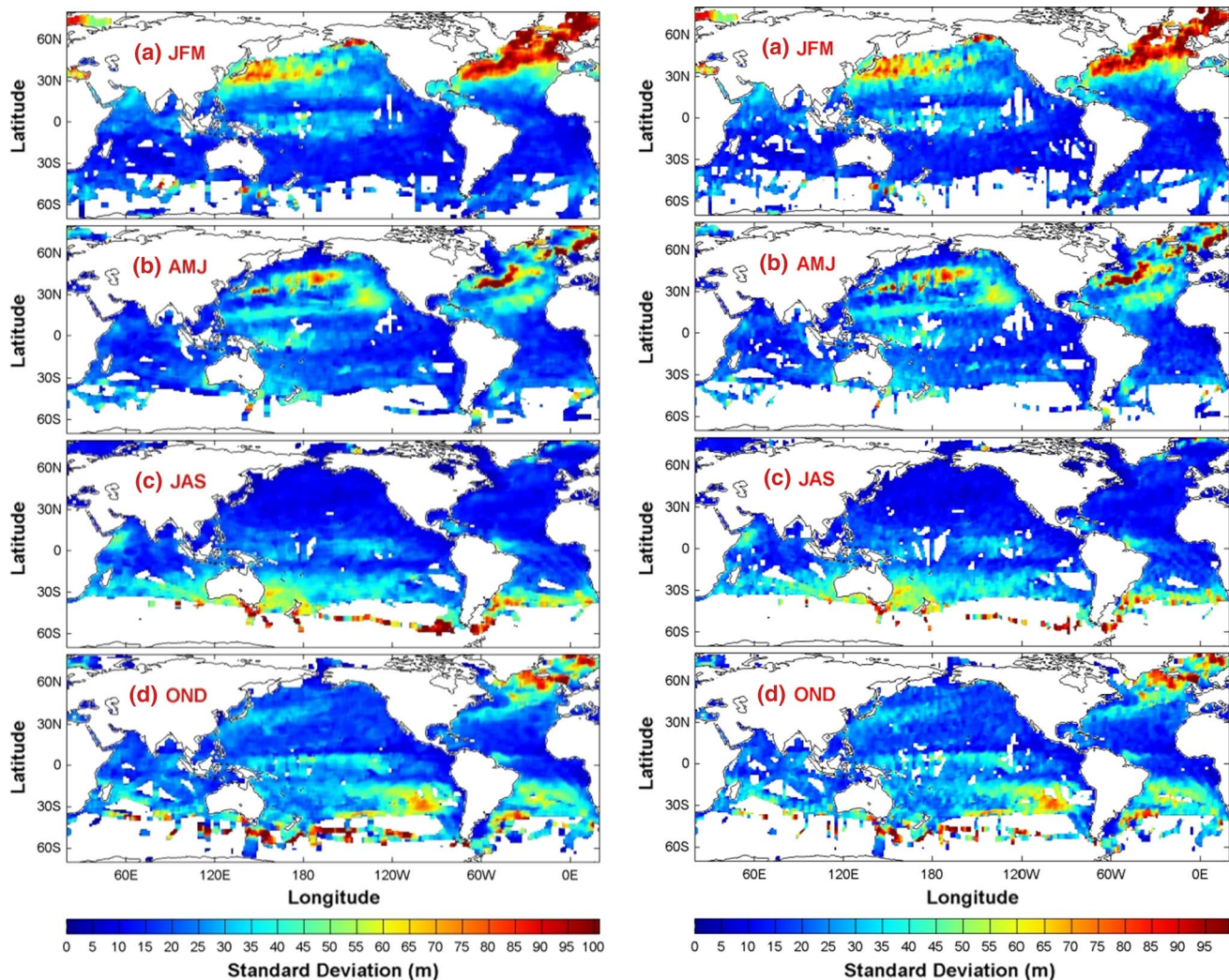
Fig. 4 Seasonal maps (1° × 1° resolution) of the standard deviation of the isothermal layer depth (in meters, identified by the ELG method) calculated in moving 5° × 5° (*left panel*) and 3° × 3° (*right panel*) grid boxes and evaluated at the centers of the boxes: **a** Janu-

ary–February–March, **b** April–May–June, **c** July–August–September, and **d** October–November–December. *White regions* have undefined values due to the presence of insufficient data points (≤4 points) in the 5° × 5° (or 3° × 3°) grid box

summer (JAS for the Northern Hemisphere, Fig. 4c; JFM for the Southern Hemisphere, Fig. 4a).

Maps of the skewness of H_T (Fig. 5) show more positive than negative values (prevailing positive skewness). The skewness presents weaker seasonal variation in the tropics than outside them. Outside the tropics, a vast area of high positive skewness (>1.4) occurs in hemispheric spring, smaller areas of alternate positive–negative skewness appear in hemispheric fall (Fig. 5b, d), and small areas of alternate positive–negative skewness occur in winter (JFM) and summer (JAS). In the tropics, alternate positive–negative skewness occurs year-round with weak seasonal variation.

The kurtosis of H_T (Fig. 6) exhibits large values (>6) in spring and a band structure along boundary currents such

as the Kuroshio and Gulf Stream (AMJ, Fig. 6b), as well as an eddy-like structure west of Australia at around 30°S (OND, Fig. 6d). The kurtosis shows weaker seasonal variations in the tropics than outside them, where low kurtosis (<3.0) occurs in fall and high kurtosis in spring (Fig. 6b, d).

6 Dynamical implications of the statistical parameters

Two distinct patterns in the mean, standard deviation, skewness, and kurtosis of the ILD are observed: weak seasonal variability in the tropics and strong seasonal variability outside them. These patterns are related to differences between these regions in their mixed-layer
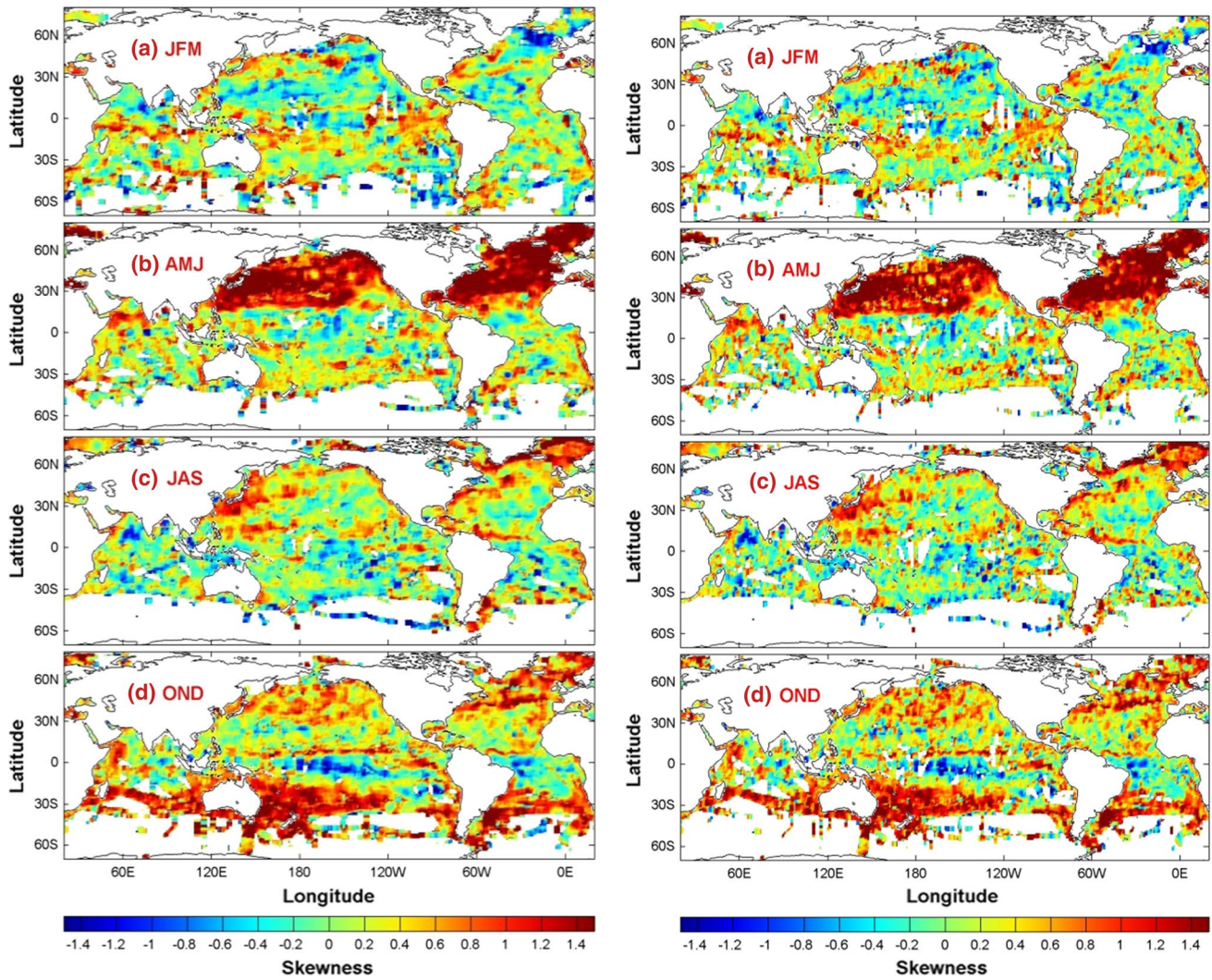
Fig. 5 Seasonal maps ($1° \times 1°$ resolution) of the skewness of the isothermal layer depth (identified by the ELG method) calculated in moving $5° \times 5°$ (*left panel*) and $3° \times 3°$ (*right panel*) grid boxes and evaluated at the centers of the boxes: **a** January–February–March, **b** April–May–June, **c** July–August-September, and **d** October–November–December. *White regions* have undefined values due to the presence of insufficient data points (≤ 4 points) in the $5° \times 5°$ (or $3° \times 3°$) grid box

deepening (entrainment) and shallowing regimes, as determined by the surface forcing function (e.g., Chu and Garwood 1991; Chu 1993):

$$F = \Lambda(C_1 w_*^3 - C_2 \alpha g H_T Q_0), \tag{17}$$

where w_* is the ocean friction velocity (representing the surface wind stress), g is the gravitational acceleration, α is the thermal expansion coefficient, Q_0 is the surface heat flux (positive in the downward direction), C_1 ($\simeq 1.0$) and C_2 ($\simeq 0.2$) are tuning parameters, and Λ is the Heaviside function of $(C_1 w_*^3 - C_2 \alpha g H_T Q_0)$,

$$\Lambda = \begin{cases} 1, & \text{if } (C_1 w_*^3 - C_2 \alpha g H_T Q_0) > 0 \\ 0, & \text{if } (C_1 w_*^3 - C_2 \alpha g H_T Q_0) \leq 0 \end{cases} \tag{18}$$

When $\Lambda = 1$, sufficient turbulent kinetic energy is generated at the surface (strong surface forcing) to entrain water from below into the mixed layer, thus deepening this layer (entrainment regime). The deepening rate is proportional to the surface forcing function F. When $\Lambda = 0$, the turbulent kinetic energy generated at the surface is insufficient (weak surface forcing) to entrain water from below into the mixed layer, causing the depth of this layer to decrease (shallowing regime) to the Obukhov length scale L,

$$H_T = L = \frac{C_1 w_*^3}{C_2 \alpha g Q_0}. \tag{19}$$

There is strong seasonal variability in surface forcing in non-tropical regions, with strong heat loss at the
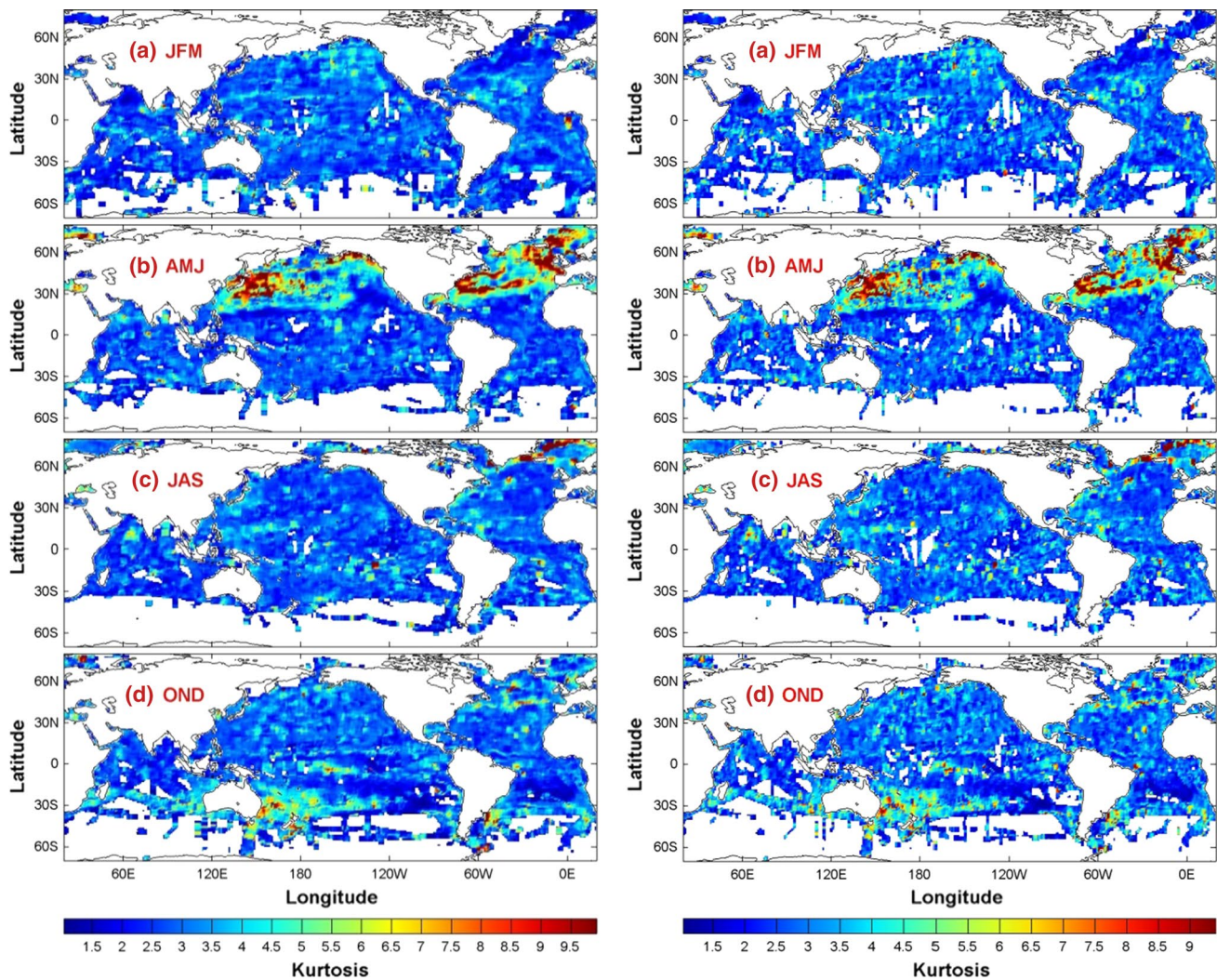
Fig. 6 Seasonal maps (1° × 1° resolution) of the kurtosis of the isothermal layer depth (identified by the ELG method) calculated in moving 5° × 5° (*left panel*) and 3° × 3° (*right panel*) grid boxes and evaluated at the centers of the boxes: **a** January–February–March, **b** April–May–June, **c** July–August–September, and **d** October–November–December. *White regions* have undefined values due to the presence of insufficient data points (≤4 points) in the 5° × 5° (or 3° × 3°) grid box

surface ($Q_0 < 0$, upward heat flux) in hemispheric winter (i.e., strong surface forcing) and strong heat gain at the surface ($Q_0 > 0$, downward heat flux) in hemispheric summer (weak surface forcing). Strong surface forcing (large F) deepens the ILD (entrainment regime) and leads to a large mean ILD and negative skewness (a long tail towards small ILD, i.e., high probability in large ILD bins). Weak surface forcing decreases the ILD (shallowing regime) and leads to a small mean ILD and positive skewness (a long tail towards large ILD, i.e., high probability in small ILD bins). During the transition from winter (summer) to summer (winter), the surface forcing changes, leading to a shift from the deepening (shallowing) to the shallowing (deepening) regime, which increases the variability and leads to large standard deviation and kurtosis values. Tropical regions show weak seasonal variability in the surface forcing function, and thus present less seasonal variation in the statistical

Fig. 7 a Thermal parametric model consisting of the isothermal layer, the thermocline, and the deep layer. **b** Discrete analytical profile (see Eq. 20) corresponding to the parameters given in Eq. 21 and the vertical resolution given in Eq. 22
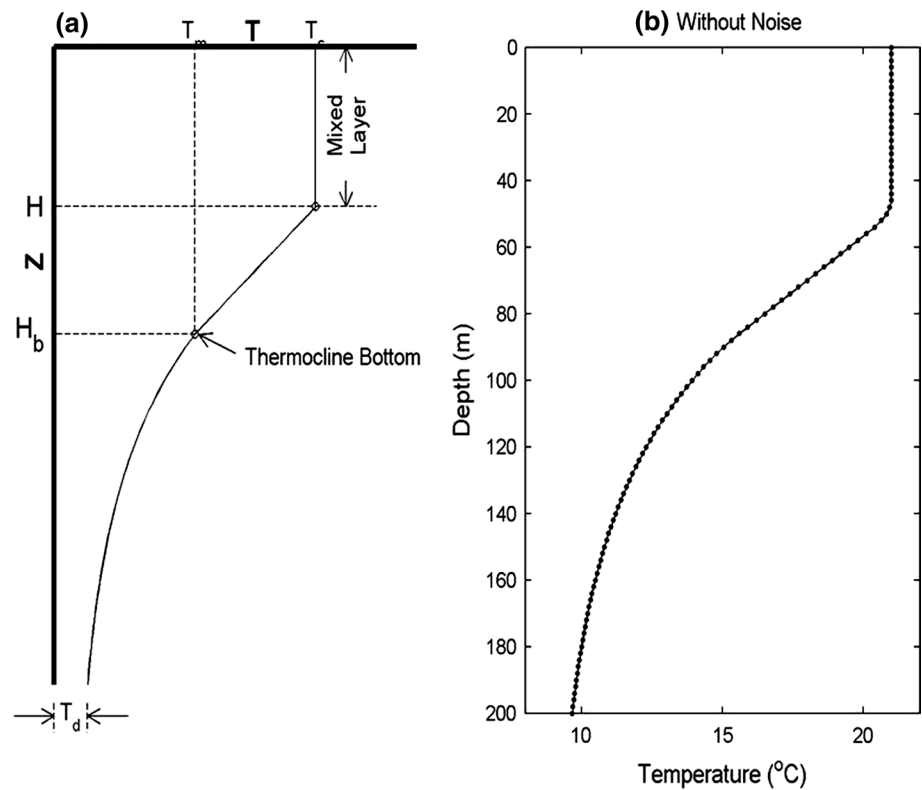
parameters (mean, standard deviation, skewness, and kurtosis of the ILD).

7 Conclusions

We have utilized the skill score and Shannon information entropy to evaluate the abilities of five existing methods (difference and gradient methods with various criteria, maximum curvature, maximum angle, optimal linear fitting) to identify the ILD (H_T) based on the WOD/CTD temperature (1961–2012, 847,560 profiles) and global GTSPP/XBT (1990–2013, 572,504 profiles) datasets, as well as the uncertainty associated with each method. Using 0.75 as the threshold for the skill score, the most useful existing methods were found to be the difference method with criteria of $\Delta T = 0.2$ °C, $z_{ref} = -10$ m for the GTSPP/XBT data, the gradient method with a criterion of 0.025 °C/m for the WOD/

CTD data, the maximum angle method for the WOD/ CTD data, and the OLF method for both the GTSPP/ XBT and WOD/CTD datasets.

We also proposed a new exponential leap-forward gradient (ELG) scheme for determining H_T with low uncertainty. Compared with the existing methods mentioned above, the ELG scheme yielded a higher skill score and lower Shannon information entropy. The global H_T data obtained by applying the ELG method showed strong horizontal and seasonal variability. The calculated statistical parameters (the mean, standard deviation, skewness, and kurtosis of the ILD) exhibited strong seasonal variability in non-tropical regions, with large mean ILD values and negative skewness (a long tail towards small ILD, i.e., high probability in large ILD bins) in hemispheric winter, small mean ILD values and positive skewness (a long tail towards large ILD, i.e., high probability in small ILD bins) in hemispheric summer, and large values of standard deviation
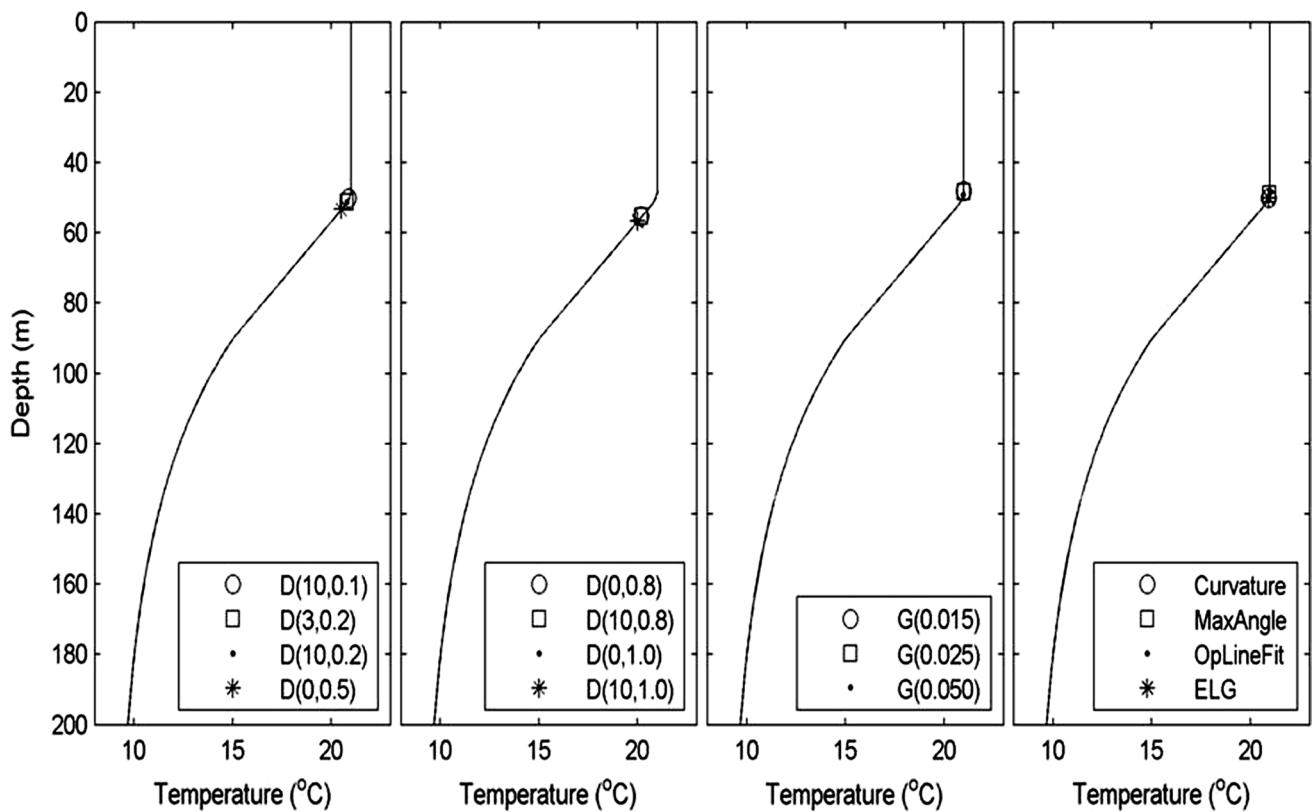
Fig. 8 Comparison of the ILD values given by the various ILD identification methods when they were applied to the analytical profile defined in Eqs. 20–22: **a** difference method with $\Delta T = 0.1$, 0.2, and 0.5 °C; **b** difference method with $\Delta T = 0.8$ and 1.0 °C; **c** gradient method with $\partial T/\partial z = 0.015$, 0.025, 0.05 °C/m; **d** maximum curvature, maximum angle, optimal linear fitting, and ELG methods

Table 3 Determination of ILD (m) from the noiseless analytical profile and from analytical profiles with two levels of Gaussian white noise added (0.05, 0.2 °C)

Method	$-z_{ref}$ (m)	Isothermal layer depth (m)		
		From analytical profile with no noise	From analytical profiles with white noise	
			White noise strength: 0.05 °C	White noise strength: 0.2 °C
(1) $\Delta T = 0.1$ °C	10	50.1	49.4	12.8
(2) $\Delta T = 0.2$ °C	3	51.2	50.8	37.9
(3) $\Delta T = 0.2$ °C	10	51.2	50.5	16.3
(4) $\Delta T = 0.5$ °C	0	53.3	53.3	53.2
(5) $\Delta T = 0.8$ °C	0	55.3	55.3	55.4
(6) $\Delta T = 0.8$ °C	10	55.3	55.1	54.2
(7) $\Delta T = 1.0$ °C	0	56.7	56.7	57.0
(8) $\Delta T = 1.0$ °C	10	56.7	56.5	56.1
(9) $\partial T/\partial z = 0.015$ °C/m		48.0	4.5	4.5
(10) $\partial T/\partial z = 0.025$ °C/m		48.3	4.5	4.5
(11) $\partial T/\partial z = 0.05$ °C/m		49.2	48.8	4.5
(12) Maximum curvature		50.0	19.0	19.0
(13) Maximum angle		49.0	48.0	35.0
(14) Optimal linear fitting		48.0	50.0	52.0
(15) ELG		50.0	51.0	49.0

The ILD of the analytical profile was 50 m
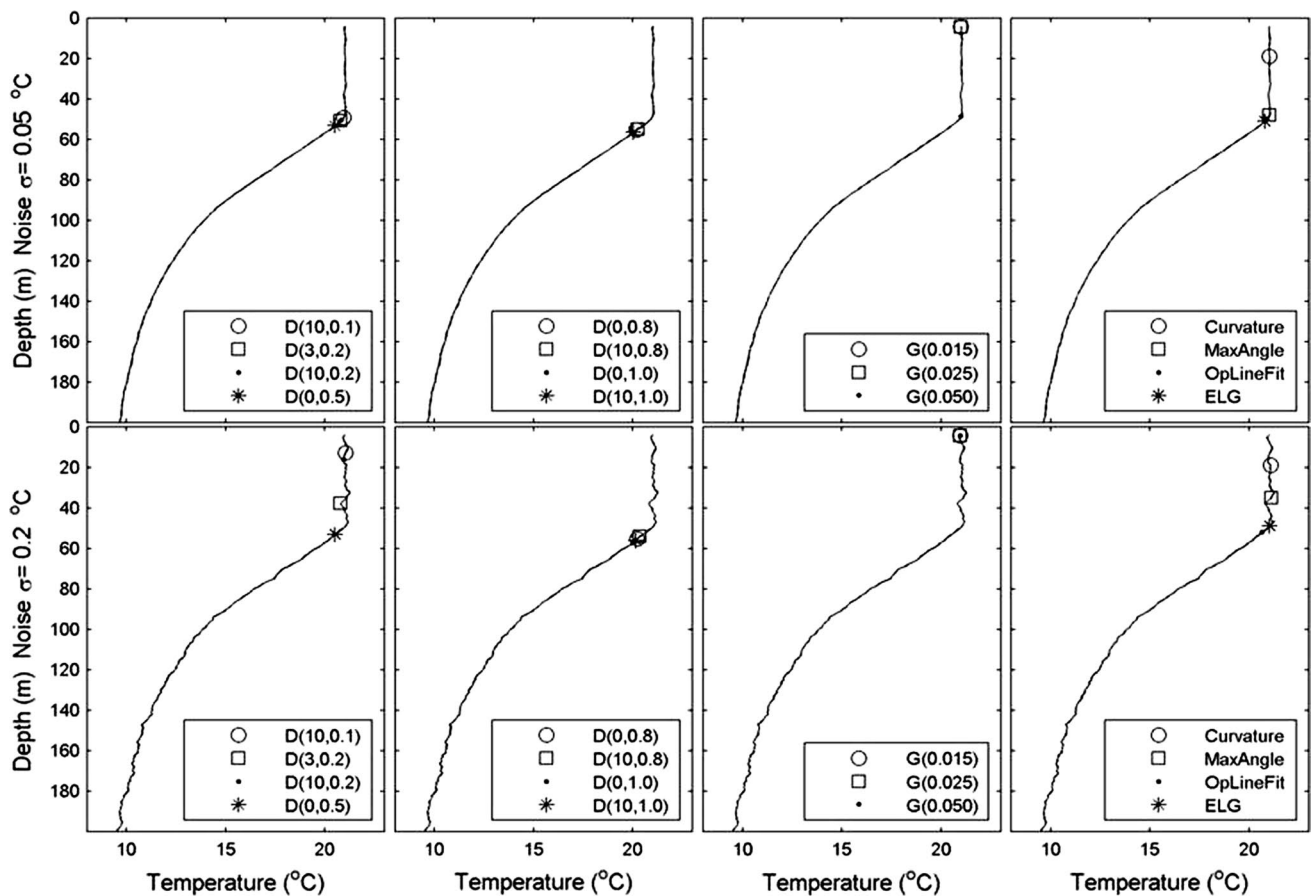
Fig. 9 Comparison of the ILD values given by the various identification methods when they were each applied to the analytical profile defined in Eqs. 20–22 with added low-level (0.05 °C) Gaussian white noise (*upper panels*) or added high-level (0.2 °C) Gaussian white noise (*lower panels*): **a** difference method with $\Delta T = 0.1$, 0.2, and 0.5 °C; **b** difference method with $\Delta T = 0.8$ and 1.0 °C; **c** gradient method with $\partial T/\partial z = 0.015$, 0.025, 0.05 °C/m; **d** maximum curvature, maximum angle, optimal linear fitting, and ELG methods. Note that only one profile with low-level noise (i.e., 1 realization) and one profile with high-level noise (1 realization) was analyzed by each method

and kurtosis during the transition seasons due to strong seasonal variability of the surface forcing function, which leads to switching between the deepening and shallowing regimes. However, the statistical parameters presented weak seasonal variability in tropical regions due to weak seasonal variability in the surface forcing function. Furthermore, the calculated skewness and kurtosis showed non-Gaussian statistics for the ILD in the global ocean.

It should be noted that the isothermal (mixed) layer is considered to be vertically uniform in temperature (density), and the isothermal layer depth is generally larger than the mixed layer depth in the subarctic region. In other words, the salinity significantly influences the MLD in the subarctic region. There are areas where a mixed layer forms under the influence of both temperature and salinity even when there are no isothermal and isohaline layers. Therefore, numerous studies have been

Fig. 10 Histograms of ILD values obtained by applying each of the 15 ILD-determination methods to the 1000 profiles with added low-level (0.05 °C) Gaussian white noises (1000 realizations) added to the analytical profile (20)-(22). The mean and standard deviation of H_T for each method are listed in the corresponding panels
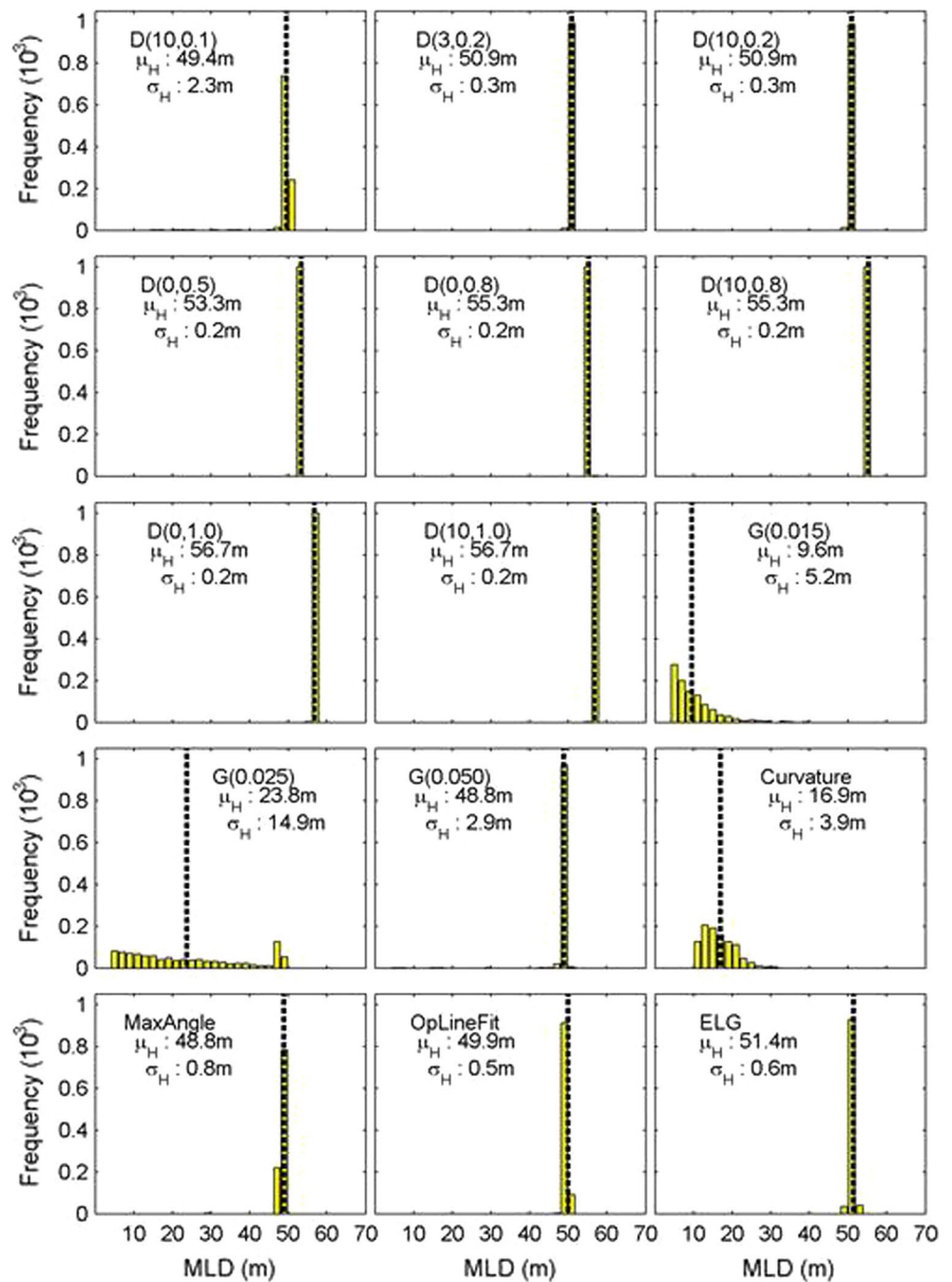
Fig. 11 Histograms of ILD values obtained by applying each of the 15 ILD-determination methods to the 1000 profiles with added high-level (0.2 °C) Gaussian white noises (1000 realizations) added to the analytical profile (20)-(22). The mean and standard deviation of H_T for each method are listed in the corresponding panels
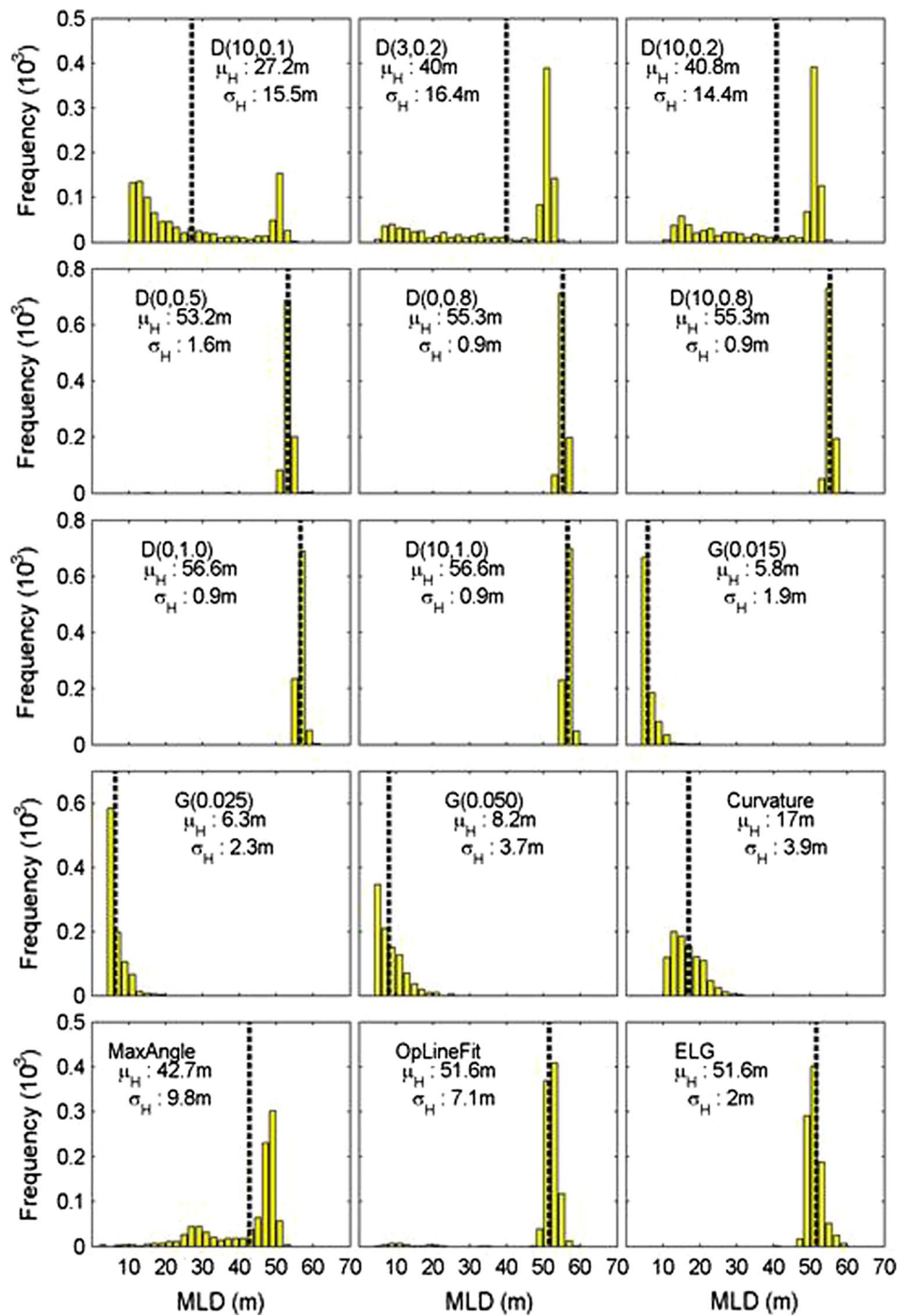
Fig. 12 Histograms of Q values obtained by applying each of the 15 ILD-determination methods to the 1000 profiles with added low-level (0.05 °C) Gaussian white noises (1000 realizations) added to the analytical profile (20)-(22). The mean and standard deviation of Q for each method are listed in the corresponding panels
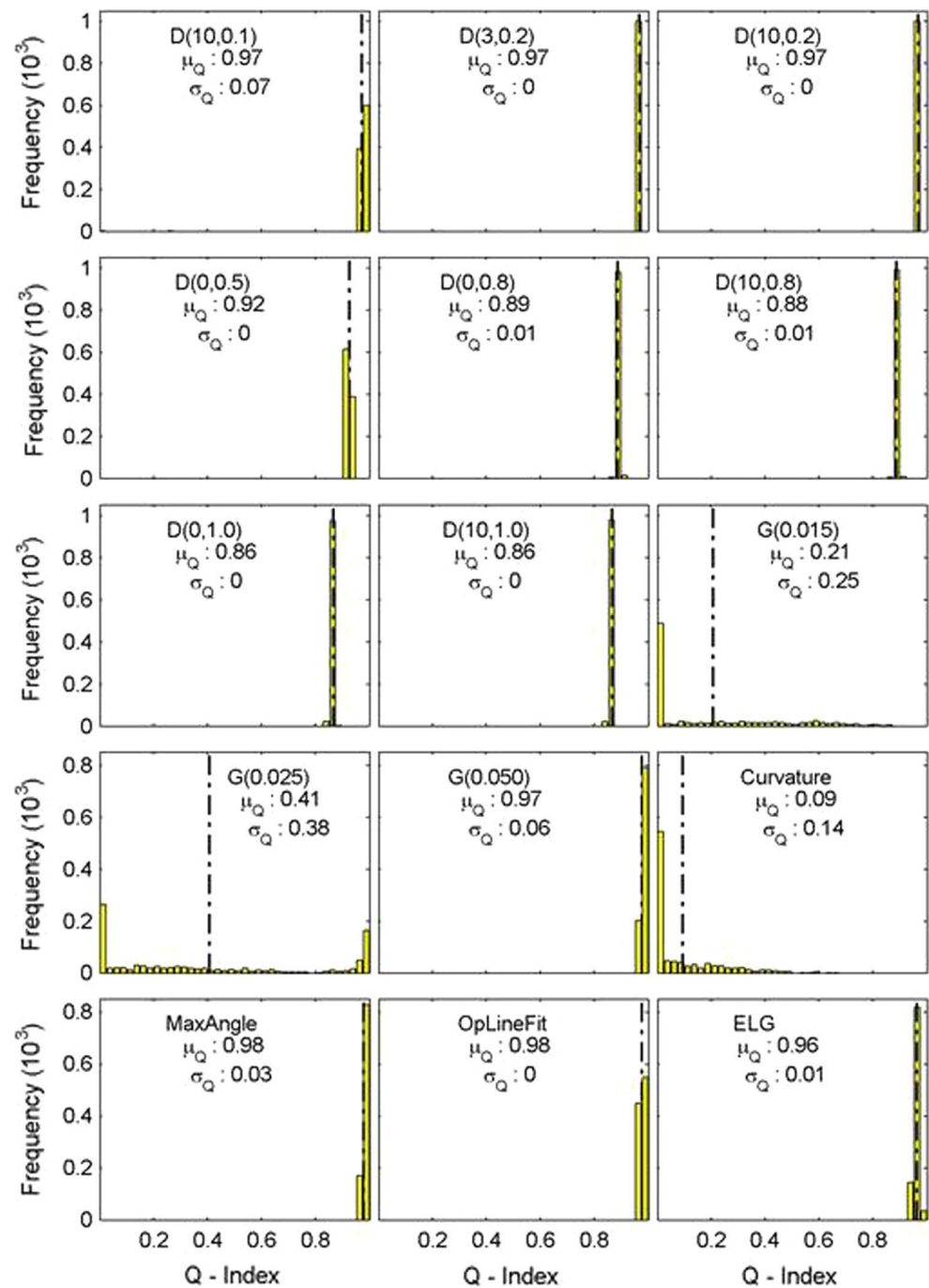
Fig. 13 Histograms of Q values obtained by applying each of the 15 ILD-determination methods to the 1000 profiles with added high-level (0.2 °C) Gaussian white noises (1000 realizations) added to the analytical profile (20)-(22). The mean and standard deviation of Q for each method are listed in the corresponding panels
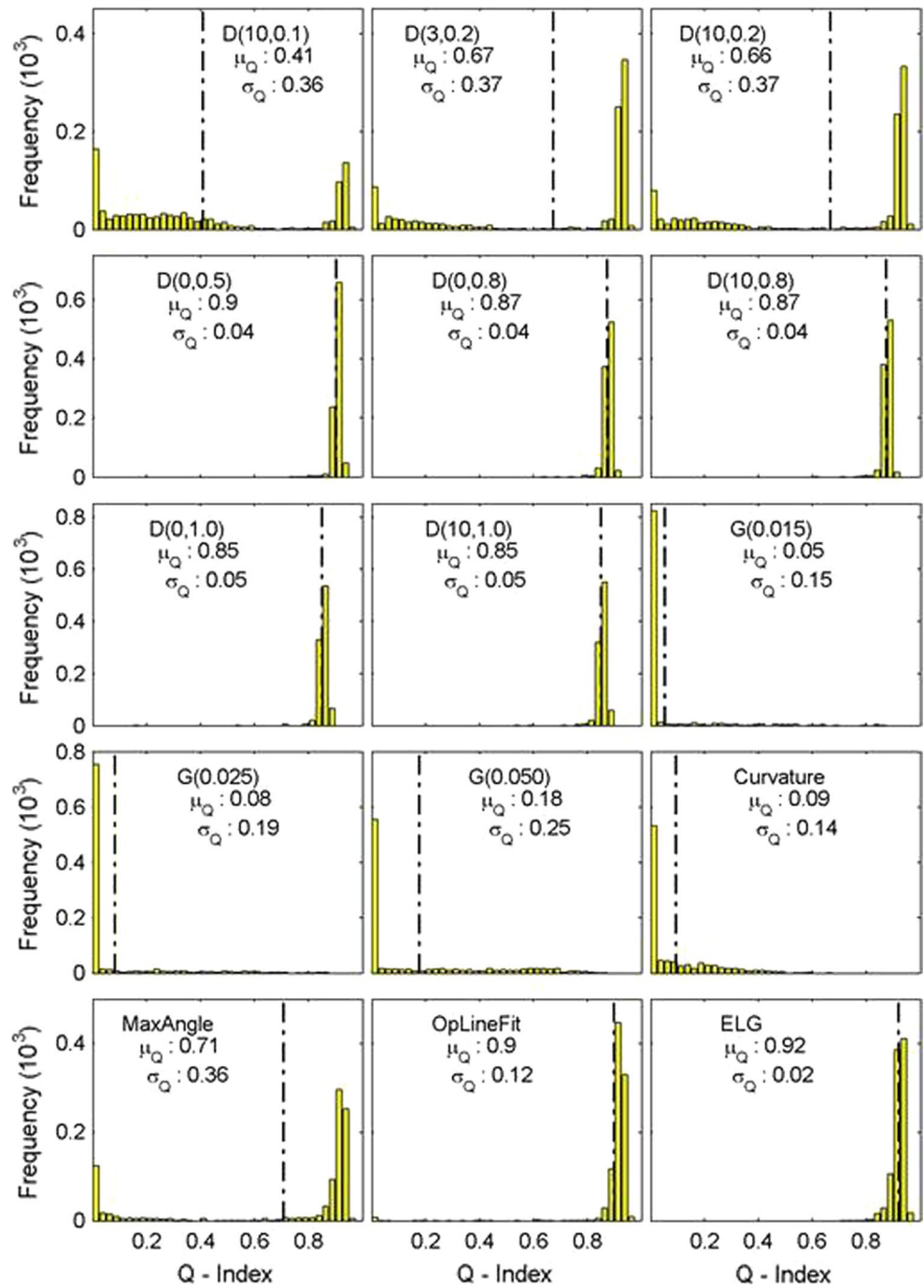
Table 4 Values for the mean ILD (m), Q index, and Shannon information entropy E_Q obtained when 15 ILD-determination methods were applied to the 1000 profiles with low-level (0.05 °C) Gaussian white noises (1000 realizations) added to the analytical profile (20)-(22)

Method	$-z_{ref}$ (m)	μ_H (m)	μ_Q	E_Q
(1) $\Delta T = 0.1$ °C	10	49.4	0.97	0.73
(2) $\Delta T = 0.2$ °C	3	50.9	0.97	0.01
(3) $\Delta T = 0.2$ °C	10	50.9	0.97	0
(4) $\Delta T = 0.5$ °C	0	53.3	0.92	0.67
(5) $\Delta T = 0.8$ °C	0	55.3	0.89	0.11
(6) $\Delta T = 0.8$ °C	10	55.3	0.88	0.08
(7) $\Delta T = 1.0$ °C	0	56.7	0.86	0.13
(8) $\Delta T = 1.0$ °C	10	56.7	0.86	0.11
(9) $\partial T/\partial z = 0.015$ °C/m		9.6	0.21	2.46
(10) $\partial T/\partial z = 0.025$ °C/m		23.8	0.41	2.94
(11) $\partial T/\partial z = 0.05$ °C/m		48.8	0.97	0.56
(12) Maximum curvature		16.9	0.09	2.01
(13) Maximum angle		48.8	0.98	0.47
(14) Optimal linear fitting		49.9	0.98	0.69
(15) ELG		51.4	0.96	0.57

Table 5 Values for the mean ILD (m), Q indices, and Shannon information entropy E_Q obtained when 15 ILD-determination methods were applied to the 1000 profiles with high-level (0.2 °C) Gaussian white noises (1000 realizations) added to the analytical profile (20)-(22)

Method	$-z_{ref}$ (m)	μ_H (m)	μ_Q	E_Q
(1) $\Delta T = 0.1$ °C	10	27.2	0.41	3.05
(2) $\Delta T = 0.2$ °C	3	40.0	0.67	2.25
(3) $\Delta T = 0.2$ °C	10	40.8	0.66	2.37
(4) $\Delta T = 0.5$ °C	0	53.2	0.90	0.94
(5) $\Delta T = 0.8$ °C	0	55.3	0.87	1.05
(6) $\Delta T = 0.8$ °C	10	55.3	0.87	1.01
(7) $\Delta T = 1.0$ °C	0	56.6	0.86	1.13
(8) $\Delta T = 1.0$ °C	10	56.6	0.86	1.11
(9) $\partial T/\partial z = 0.015$ °C/m		5.9	0.05	0.96
(10) $\partial T/\partial z = 0.025$ °C/m		6.3	0.08	1.32
(11) $\partial T/\partial z = 0.05$ °C/m		8.2	0.18	2.17
(12) Maximum curvature		17	0.09	2.00
(13) Maximum angle		42.7	0.71	2.20
(14) OLF		51.6	0.90	1.39
(15) ELG		51.6	0.92	1.27

carried out to determine the MLD using both temperature and salinity (e.g., the identification of the barrier layer in the Sulu and Celebes seas; Chu et al. 2002). Thus, determined MLD values should be interpreted carefully, taking into account aspects such as differences in ocean structure between the tropical, subtropical, and subarctic regions.

Appendix 1: MATLAB function for computing G_{th} and preparing for ELG

```
function [ist,slop17,i17,dep,Var,isteps,I30,flag]=getslop17(dep,Var,TD)
% function [ist,slop17,i17,dep,Var,isteps,I30,flag]=getslop17(dep,Var,TD);
% Var:  variable (potential density, temperature)
% TD:   1; density, -1:temperature
% output:
% ist: an integer i with  z_i = z_1 in Eq(2)
% slop17:  G_th between z_(0.1) and z_(0.7)  in Eq(3)
% i17:   all integers {k} from z_(0.1) to  z_(0.7)  in Fig. 1
% dep:  depth (m) >0
% data pairs (dep, Var) must be removed if diff(dep)<=0
% isteps:  N+1 integers 2^0, 2, …, 2^N in Eq(14)
% flag: 0: normal
%       1: few (<=2) observational points from 10 m to 40 m
%       2: total observational points <=5
%       3: maximum  depth <20 m
%       4: starting point with depth deeper than 50 m
%       5: difference above 20 m >  different below 20 m
%       6: maximum difference < 1.0°C (temp) or < 0.01 kg/m^3 (dens)
%       7: no thermocline
%       8: thermocline gradient is too small (<0.001°C/m)
%       9: two neighboring profiles have big difference  (>5°C)

if ~exist('TD','var'), TD=-1; end

slop17=[]; i17=[]; isteps=[]; ist=[]; I30=[]; flag=0;

if max(abs(diff(Var)))>5
   flag=9; return;
end

Isteps=2.^(0:6)+1;

%Var=Var(dep>3); dep=dep(dep>3);
ii=find(dep<=800); dep=dep(ii); Var=Var(ii);
ii=find(diff(dep)<=0);
while(~isempty(ii))
   dep(ii)=[]; Var(ii)=[];
   ii=find(diff(dep)<=0);
end
Varr=Var*TD;

% if the data not good and return
if length(dep)<6, flag=2; return; end
if dep(end)<20, flag=3; return; end
if dep(1)>50, flag=4; return; end
max20=max(Varr(dep<20))-min(Varr(dep<20));
maxdeep=max(Varr(dep>20))-min(Varr(dep>20));

if max20>maxdeep, flag=5; return; end

%N=length(dep);

% set the start depth as the minimum slope above 20m depth.M
ii=find(dep<20);
if(length(ii)>2)
   slp=abs(diff(Varr(ii))./diff(dep(ii)));
   [~,ist]=min(slp);
else
   ist=1;
end
```

Appendix 2: MATLAB function for determining ILD using the ELG scheme

```
Vist=Varr(ist);
Varr=Varr-Vist;
[Vmax,imax]=max(Varr(ist:end));
imax=imax-1+ist;

% estimate the number of data points in thermocline (pycnocline)

if((Vist<40 && Vmax<=1) || (Vist>40 && Vmax<=0.01)), ist=[]; flag=6; return; end

i17=(find(Varr(ist:imax)<0.1*Vmax,1,'last'):find(Varr(ist:imax)>=0.7*Vmax,1))+ist-1;

I30=find(Varr(ist:end)>=0.3*Vmax,1)+ist-1;

if(isempty(i17)), ist=[]; flag=7; return; end

n17=length(i17);

isteps=Isteps(Isteps<=n17);
if isteps(end)<32 && isteps(end)~=n17
    isteps=cat(2,isteps,n17);
end
Nsp=length(isteps);

vv=Varr(i17(1)+1:end)-Varr(i17(1));
dd=dep(i17(1)+1:end)-dep(i17(1));
ii=find(dd>=2);
if length(ii)>3
    slop17=vv(ii)./dd(ii);
else
    slop17=vv./dd;
end

slop17=prctile(slop17,50);

if((Vist<40 & slop17<1e-3) | (Vist>=40 & slop17<1e-5)), ist=[]; flag=8; return; end

% Nsp=min(Nsp,5);
% isteps=isteps(1:Nsp)-1;

% update ist
vv=Varr(1:i17(1));
dv=abs(vv-mode(vv)); dv=dv(end:-1:1);
[~,ist]=min(dv); ist=length(dv)+1-ist;

if sum(dep>=10 & dep<=40)<2, flag=1; end
```

Appendix 3: Analytical profile "dataset" for practicing the application of the MATLAB functions

```
function [mld,Ii,Q,Vmld]=ELGMLDCore(dep,Var,ist,slop17,i17,isteps,TD)
% function [mld,Ii,Q,Vmld]=ELGMLDCore(dep,Var,ist,slop17,i17,isteps,TD);
% input:
% The input (dep,Var,ist,slop17,i17,isteps) are obtained from the output
% of the Matlab function depicted in Appendix A.
% TD: temp:-1,  density: +1

% output:
% mld:  mixed layer depth (m)
% Ii:    identification index
% Q:    qulity index
% Vmld: variable (temperature, density, …) at the mixed layer depth such as T_H

if ~exist('TD','var'), TD=-1; end
mld=NaN; Q=NaN; Vmld=NaN; Ii=NaN;

Var=TD*Var;

if isempty(ist), return; end
N=length(dep);

refslop=0.5*slop17;
n17=length(i17);

for i=ist:length(dep)-isteps(end)

   slops=(Var(i+isteps)-Var(i))./(dep(i+isteps)-dep(i));

    if min(slops)>=refslop
      mld=dep(i); Vmld=TD*Var(i);
      i15mld=find(dep<=1.5*mld);
      i3=i15mld(i15mld<=i+n17);
      i1=(1:i)';
      A1=sum((Var(i1)-mean(Var(i1))).^2);

      i2=i3(i3>i);

      if(length(i2)<3), A2=0;
      else
         p2=polyfit(dep(i2),Var(i2),1);
         v2=polyval(p2,dep(i2));
         A2=sum((Var(i2)-v2).^2);
      end

      if(length(i3)>=3)
         p3=polyfit(dep(i3),Var(i3),1);
         v3=polyval(p3,dep(i3));
         A3=sum((Var(i3)-v3).^2)+eps;
         Ii=max(-1,1-(A1+A2)/A3);
      end

      N1=i-1;
      i2=find(dep<=1.5*mld);
      N2=length(i2)-1;
```

```
    if(N2<=0)
        i2=(i:min(i+1,N))';
        N2=length(i2)-1;
    end
    if(N2==0 || N1==0)
        return;
    end
    mu=mean(Var(i1));
    A1=std(Var(i1)-mu);
    A2=std(Var(i2)-mu)+eps;
    if(A2==0), disp([mu,N2]); disp([i2, Var(i2)]); 'RG';  return; end
    Q=1-A1/A2;
%       if(Q<=0), Q=NaN; mld=NaN; end
    return;
    end
end
```

Analytical temperature profile "data"

Let us consider a temperature profile $[T(z_k), k = 1, 2, \ldots, K]$. Here, k increases downward, with $k = 1$ at the surface (or nearest to the surface) and K being the number of the data points in the profile. The ILD (i.e., H_T) is determined based on the theory that the upper ocean has a layered structure (isothermal layer, thermocline, and deep layer) (Fig. 7) and that the temperature profile $[T(z_k), k = 1, 2, \ldots, K]$ can be represented by several parameters representing the features of the profile (Chu et al. 1997, 1999, 2000), such as the sea surface temperature (T_s), the ILD, the thermocline bottom depth (H_b), the deep layer e-folding scale (H_e), the thermocline temperature gradient (G_{th}), and the deep temperature (T_d). A simple analytical form of a temperature profile is (Chu et al. 2000)

$$\tilde{T}(z) = \begin{cases} T_s, & (0 \geq z \geq -H_T) \\ T_s + G_{th}(z + H_T), & (-H_T \geq z \geq -H_b) \\ T_d + (T_{th} - T_d) \exp\left[\frac{z+H_b}{H_e}\right], & (z < -H_b) \end{cases} \quad (20)$$

where $T_{th} = T_s - G_{th}(H_b - H_T)$ is the temperature at the thermocline bottom ($z = -H_b$). T_d is the deepest ocean depth (5500 m in the NOAA/NECI climatological data); for shallow-water regions, this is obviously not a real observed value but the value obtained by extrapolating to the deepest depth (e.g., 5500 m). Any temperature

An analytical temperature profile "dataset" with regular vertical spacing is provided here as a means to practice using the MATLAB functions shown in Appendices 1 and 2.

profile $[(T(z_1), T(z_2), \ldots, T(z_K)]$ is converted into a set of seven parameters $[T_s, T_{th}, T_d, H_T, H_b, H_e, G_{th}]$. This approach has several major benefits: (a) it reduces the profile dataset (which is usually large) to a seven-parameter dataset; (b) it constructs a climatological temperature dataset by first averaging each parameter and then substituting the seven averaged parameters into Eq. 20; and (c) it eliminates any false static instability when calculating the horizontal (or temporal) averaged vertical profile (Chu and Fan 2010a; Wang et al. 2012). In practice, the parameters are

$$H_T = 50 \text{ m}, H_b = 40 \text{ m}, H_e = 200 \text{ m}, G_{th}$$
$$= 0.25° \text{ C m}^{-1}, T_s = 21°C, T_d = 2°C, \quad (21)$$

and the vertical coordinate z is discretized as follows:

$$\Delta z = \begin{cases} 1.0 \text{ m for } 0 \geq z \geq -10 \text{ m} \\ 5.0 \text{ m for } z < -10m \end{cases} \quad (22)$$

Added noise

White Gaussian noise with a magnitude of 0.05 °C (low noise) or 0.2 °C (high noise), generated by MATLAB, was added to the discrete analytical profile $T(z_k)$ at each depth 1000 times, resulting in 1000 temperature profiles. When the difference method was applied to these profiles with two different criteria, $\Delta T = 0.2$ °C with $z_{ref} = 0$ and $\Delta T = 0.2$ °C with $z_{ref} = -3$ m (Thompson 1976), both difference criteria were found to yield almost the same results.

When applied to the profile without noise, all 15 methods found H_T to be quite close to 50 m (Fig. 8). The H_T values determined using the difference method with various criteria were larger than 50 m: 50.1 m with $\Delta T = 0.1$ °C,

51.2 m with $\Delta T = 0.2$ °C, 53.3 m with $\Delta T = 0.5$ °C, 55.3 m with $\Delta T = 0.8$ °C, and 56.7 m with $\Delta T = 1.0$ °C. The ILD was smaller than 50 m when the gradient method was used with various criteria: 48.0 m for 0.015 °C/m, 48.3 m for 0.025 °C/m, and 49.2 m for 0.05 °C/m. An H_T value of 50.0 m was given by the ELG and maximum curvature methods, 49.0 m by the maximum angle method, and 48.0 m by the optimal linear fitting method (Table 3).

Applying each ILD identification method to one of the low-noise (0.05 °C) profiles (i.e., to 1 realization) and one of the high-noise (0.2 °C) profiles resulted in a wide range of H_T values (Fig. 9). When the low-noise profile was used, the H_T identified using the difference method was quite close to 50 m with $\Delta T = 0.1$, 0.2, and 0.5 °C, and 5–6 m deeper at 55 m with $\Delta T = 0.8$ and 1.0 °C. When the gradient method was used, H_T was close to 5 m for small gradients (0.015, 0.025 °C/m) and close to 50 m for a large gradient (0.05 °C/m). H_T was 19 m when the maximum curvature method was used and around 50 m when the maximum angle, OLF, and ELG methods were employed. When the high-noise profile was used, the H_T identified using the difference method was around 56 m with $\Delta T = 0.5$, 0.8, and 1.0 °C, 40 m with $\Delta T = 0.2$ °C, and 12 m with $\Delta T = 0.1$ °C. When the gradient method was used, H_T was close to 5 m (for all gradients: 0.015, 0.025, and 0.05 °C/m); it was 19 m using the maximum curvature method, 35 m using the maximum angle method, 52 m using the optimal linear fitting method, and 49 m using the ELG method.

Q values were obtained for each method with each profile using Eq. 3. Since only one profile (defined by Eqs. 20–22)—with or without added noise—was used each time, the skill score (Eq. 7) was not calculated.

Histograms of H_T and Q were constructed based on the results of applying each of the 15 ILD determination methods to the 1000 low-noise profiles (i.e., 1000 realizations; see Figs. 10, 12) and to the high-noise profile (see Figs. 11, 13). The statistical results obtained for the low-noise profiles are listed in Table 4, and those obtained for the high-noise profiles are shown in Table 5.

References

Araujo M, Limongi C, Servain J, Silva M, Leite FS, Veleda D, Lentini AD (2009) Salinity-induced mixed and barrier layers in the southwestern tropical Atlantic Ocean off the northeast of Brazil. Ocean Sci 7:63–73

Cheng L, Abraham J, Goni G, Boyer T, Wijffels S, Cowley R, Gouretski V, Reseghetti F, Kizu S, Dong S, Bringas F, Goes M, Houpert L, Sprintall J, Zhu J (2016) XBT Science: assessment of instrumental biases and errors. Bull Am Meteorol Soc 97:924–933. doi:10.1175/BAMS-D-15-00031.1

Chu PC (1993) Generation of low frequency unstable modes in a coupled equatorial troposphere and ocean mixed layer. J Atmos Sci 50:731–749

Chu PC (2006) P-Vector Inverse Method, Springer, Berlin, Heidelberg, pp 11-62

Chu PC, Fan CW (2010a) A conserved minimal adjustment scheme for stabilization of hydrographic profiles. J Atmos Oceanic Technol 27:1072–1083

Chu PC, Fan CW (2010b) Optimal linear fitting for objective determination of ocean mixed layer depth from glider profiles. J Atmos Oceanic Technol 27:1893–1898

Chu PC, Fan CW (2011) Maximum angle method for determining mixed layer depth from seaglider data. J Oceanogr 67:219–230

Chu PC, Garwood RW Jr (1991) On the two-phase thermodynamics of the coupled cloud–ocean mixed layer. J Geophys Res 96:3425–3436

Chu PC, Garwood RW Jr, Muller P (1990) Unstable and damped modes in coupled ocean mixed layer and cloud models. J Mar Syst 1:1–11

Chu PC, Fralick CR, Haeger SD, Carron MJ (1997) A parametric model for Yellow Sea thermal variability. J Geophys Res 102:10499–10508

Chu PC, Wang QQ, Bourke RH (1999) A geometric model for Beaufort/Chukchi Sea thermohaline structure. J Atmos Oceanic Technol 16:613–632

Chu PC, Fan CW, Liu WT (2000) Determination of sub-surface thermal structure from sea surface temperature. J Atmos Oceanic Technol 17:971–979

Chu PC, Liu QY, Jia YL, Fan CW (2002) Evidence of barrier layer in the Sulu and Celebes Seas. J Phys Oceanogr 32:3299–3309

De Boyer Montegut C, Madec G, Fisher AS, Lazar A, Iudicone D (2004) Mixed layer depth over the global ocean: an examination of profile data and a profile-based climatology. J Geophys Res 109:C12003. doi:10.1029/2004JC002378

Defant A (1961) Physical oceanography, vol. 1. Pergamon, London

Kara AB, Rochford PA, Hurlburt HE (2000) An optimal definition for ocean mixed layer depth. J Geophys Res 105:16803–16821

Lamb PJ (1984) On the mixed layer climatology of the north and tropical Atlantic. Tellus A 36:292–305

Lorbacher K, Dommenget D, Niiler PP, Kohl A (2006) Ocean mixed layer depth: a subsurface proxy of ocean-atmosphere variability. J Geophys Res 11:C07010. doi:10.1029/2003JC002157

Lukas R, Lindstrom E (1991) The mixed layer of the western equatorial Pacific Ocean. J Geophys Res 96:3343–3357

Monterey G, Levitus S (1997) Seasonal variability of mixed layer depth for the world ocean. Technical report. NOAA, Silver Spring

Obata A, Ishizaka J, Endoh M (1996) Global verification of critical depth theory for phytoplankton bloom with climatological in situ temperature and satellite ocean color data. J Geophys Res 101:20657–20667

Oka E, Talley LD, Suga T (2007) Temporal variability of winter mixed layer in the mid-to-high latitude North Pacific. J Oceanogr 63:293–307

Rao RR, Molinari RL, Festa JF (1989) Evolution of the climatological near-surface thermal structure of the tropical Indian Ocean: 1. Description of mean monthly mixed layer depth, and sea surface temperature, surface current, and surface meteorological fields. J Geophys Res 94:10801–10815

Sprintall J, Roemmich D (1999) Characterizing the structure of the surface layer in the Pacific Ocean. J Geophys Res 104:23297–23311

Sun C (2010) GTSPP real-time quality control manual, revised edition. UNESCO, Paris. http://www.iode.org/index.php?option=com_oe&task=viewDocumentRecord&docID=6437

Sun C et al (2009) The data management system for the Global temperature and Salinity Profile Programme. In: Hall J, Harrison

DE, Stammer D (eds) Proceedings of OceanObs'09: Sustained Ocean Observations and Information for Society (vol. 2), Venice, Italy, 21–25 September 2009. ESA publ. WPP-306. ESA, Noordwijk. doi:10.5270/OceanObs09.cwp.86. http://www.oceanobs09.net/proceedings/cwp/cwp86/index.php

Thompson R (1976) Climatological numerical models of the surface mixed layer of the ocean. J Phys Oceanogr 6:496–603

Wang X, Chu PC, Han G, Li W, Zhang X, Li X (2012) A fully conserved minimal adjustment scheme with (T,S) coherency for stabilization of hydrographic profiles. J Atmos Oceanic Technol 29:1854–1865

Wyrtki K (1964) The thermal structure of the eastern Pacific Ocean. Dstch Hydrogr Zeit Suppl Ser A 8:6–84